Theor Appl Climatol (2017) 130:775–790
DOI 10.1007/s00704-016-1923-6

ORIGINAL PAPER

# The impact of climatic and non-climatic factors on land surface temperature in southwestern Romania

**Cristina Florina Roşca[1] · Gabriela Victoria Harpa[1] · Adina-Eliza Croitoru[2] · Ioana Herbel[1] · Alexandru Mircea Imbroane[3] · Doina Cristina Burada[4]**

Received: 5 March 2016 / Accepted: 24 August 2016 / Published online: 2 September 2016


**Abstract** Land surface temperature is one of the most important parameters related to global warming. It depends mainly on soil type, discontinuous vegetation cover, or lack of precipitation. The main purpose of this paper is to investigate the relationship between high LST, synoptic conditions and air masses trajectories, vegetation cover, and soil type in one of the driest region in Romania. In order to calculate the land surface temperature and normalized difference vegetation index, five satellite images of LANDSAT missions 5 and 7, covering a period of 26 years (1986–2011), were selected, all of them collected in the month of June. The areas with low vegetation density were derived from normalized difference vegetation index, while soil types have been extracted from Corine Land Cover database. HYSPLIT application was employed to identify the air masses origin based on their backward trajectories for each of the five study cases. Pearson, logarithmic, and quadratic correlations were used to detect the relationships between land surface temperature and observed ground temperatures, as well as between land surface temperature and normalized difference vegetation index. The most important findings are: strong correlation between land surface temperature derived from satellite images and maximum ground temperature recorded in a weather station located in the area, as well as between areas with land surface temperature equal to or higher than 40.0 °C and those with lack of vegetation; the sandy soils are the most prone to high land surface temperature and lack of vegetation, followed by the chernozems and brown soils; extremely severe drought events may occur in the region.

✉ Cristina Florina Roşca
cristina_rosca88@yahoo.com; cf_rosca@yahoo.com

[1] Faculty of Geography, Babeş-Bolyai University, 5-7, Clinicilor Street, 400006 Cluj-Napoca, Cluj, Romania

[2] Faculty of Geography, Department of Physical and Technical Geography, Babeş-Bolyai University, 5-7, Clinicilor Street, 400006 Cluj-Napoca, Cluj, Romania

[3] Faculty of Geography, Department of Regional Geography and Territorial Planning, Babeş-Bolyai University, 5-7, Clinicilor Street, 400006 Cluj-Napoca, Cluj, Romania

[4] Oltenia Regional Meteorological Center, National Meteorological Administration, 3A, Brestei Street, Craiova, Dolj, Romania

## 1 Introduction

Land surface temperature (LST) is one of the most important key parameters related to global warming directly (Sekertekin et al. 2016). It depends mainly on discontinuous vegetation cover that is affected by high temperature or lack of precipitation and significantly increases the vegetation phenology. The vegetation cover is affected by drought phenomenon that is present in the study area with high frequency. In terms of quantitative analysis of drought, it is largely demonstrated that it is a complex issue and it is difficult to develop a definition to describe or an index to measure it (Radinović and Ćurić 2009; Ćurić 2012). Many quantitative indices have been developed so far along tens of years (De Martonne 1926; Palmer 1965; McKee et al. 1993; Ćurić 2012; Radinović and Ćurić 2009, 2013; Vicente-Serrano et al. 2010).

Vegetation phenology is often used as a measurement tool for short- or long-term impact of climate variability. The impact of climate change on vegetation can be found in many research papers (Zhou et al. 2001; Bunn et al. 2005; White et al. 2005; Meng et al. 2011; Ćurić and Živanović 2013; Lei et al. 2014).

Normalized difference vegetation index (NDVI) is a commonly and efficiently used method to detect the vegetation

properties, including light absorption capacity and photosynthetic potential. A strong relationship between LST and vegetation indices has been found in many research studies conducted in different regions of the world (Anderson et al. 2004; Amiri et al. 2009; Chakraborthy and Sehgal 2010; Sruthi and Mohammed Aslam 2015). The climate variability affects vegetation in various ways due to a great diversity of crops and soil types. Soil type and land use change are important contributors to values of LST and NDVI. The two satellite derived products are used in this study to highlight the influence on the reflectance for different soil types and crops.

LST can highlight the local climate effects trough their changes. Usually, high LST values are closely related to lack of vegetation because combined with high air temperature, different soil types, under no irrigation conditions, significantly increase the impact on vegetation.

A commonly used method to determine the origin of an air mass is to follow its backward trajectory. Air Resources Laboratory (ARL) of NOAA's Office of Oceanic and Atmospheric Research has developed the Hybrid Single Particle Lagrangian Integrated Trajectory (HYSPLIT) model, which is a complete system for computing simple air parcel trajectories, as well as transport, dispersion, and deposition simulations. HYSPLIT has been widely used in climatic or meteorological studies (Kassomenos et al. 2010; Katarzyna 2013; Tošić and Unkašević 2013; Soltani et al. 2014; Bogawski and Bednorz 2016), for calculating air mass paths from one region to another in studies related to environmental issues (Poissant 1999; Hsu et al. 2003; Sjöstrom and Welker 2009; Djordjević et al. 2010), as well as in air pollution applications (Borge et al. 2007; Adame et al. 2015).

The main purpose of this paper is to investigate the relationship between high LST, its generating synoptic conditions and air masses origin, vegetation cover, and soil type in one of the driest region in Romania, based on five summertime case studies.

## 2 Study area

The study area is part of the Romanian Plain and is located in Southwestern Romania. It covers an area of 3904 km$^2$ and extends between 44° 20′ 01″–43° 41′ 40″ of Northern latitude and between 23° 01′ 44″–24° 32′ 33″ of Eastern longitude (Fig. 1). Usually named "Romanian Sahara", this territory has been chosen as study area because of its socioeconomic and especially climatic fragile balance.

Agricultural landscapes are prevailing, but the specificity is given by the presence of numerous sand dunes of different type: fixed, mobile, or semi-mobile. Their genesis is attributed to the Danube and Jiu Rivers in early Quaternary and more than 51 % of the considered area is covered by sandy soils (Irimus 2003).

In terms of climate, the temperate continental climate is dominant, but quite frequent the Mediterranean climate influences are present in the Southwestern Romania (Sandu et al. 2008). High values of monthly absolute maximum air temperature in the summer, measured in standard weather station conditions (35.0–43.0 °C), reference evapotranspiration higher than precipitation rate (550–700 mm/vegetation period, 100–235 mm/summer), and low precipitation over the entire year, but especially in summer (less than 549.6 mm/year, and 173.3 mm/summer season) lead to frequent drought episodes. They occur especially in the summertime when they are associated to heat waves (Roşca 2012; Croitoru et al. 2013, 2015; Burada 2013), stress the crops, and make from this area one of the most fragile in terms of agriculture use. Both temperature and reference evapotranspiration as mean multiannual value reach their highest level in the south of the region, and they decrease northward.

Climate change analysis over a 53-year period (1961–2013) revealed upward trends of air temperature and reference evapotranspiration, while rainfall indicated no significant change (Roşca 2013; Croitoru et al. 2013). Compared to the period 1961–1991, over the period 1992–2013, the highest increase in temperature as net values was detected for summer months (1.1–1.4 °C for June and 1.7–1.8 °C in August).

In terms of anthropogenic factors, over the last 30 years, in Southern Romania, there have been major changes in land use, some of them are due to the geopolitic context, while some other have been associated to climate variability. Thus, in the very next year after the communism collapse (December 1989), the legislation changed and imposed a transfer of land from common property of the state to individuals and private companies. Under these circumstances, the land division in areas smaller than 10 ha (the largest area that could be returned to one owner, according to the law) has been a long and a very time-consuming process.

Under existing natural (soil and precipitation) conditions, it is impossible to develop a sustainable and competitive agriculture without irrigation in the region. Because it is an aridity prone area, in the mid-1970s, some vegetal windbreakers were planted to protect against the moving sands and heavy blizzards, and an irrigation system was implemented in order to improve the agriculture yields and variety.

At the end of the 1990s, the high cost for operating and maintenance on the one hand, and the impossibility of individual owners to pay for water supply for plants on the other hand, led to discontinuous use of the irrigation system and then, to its gradually degradation and destruction.

Moreover, in less than one decade (2003–2010), the forested area diminished by 22.6 % (559.47 ha), while only 3.02 % of the region (64.26 ha) were afforested (Roşca and Petrea 2014).

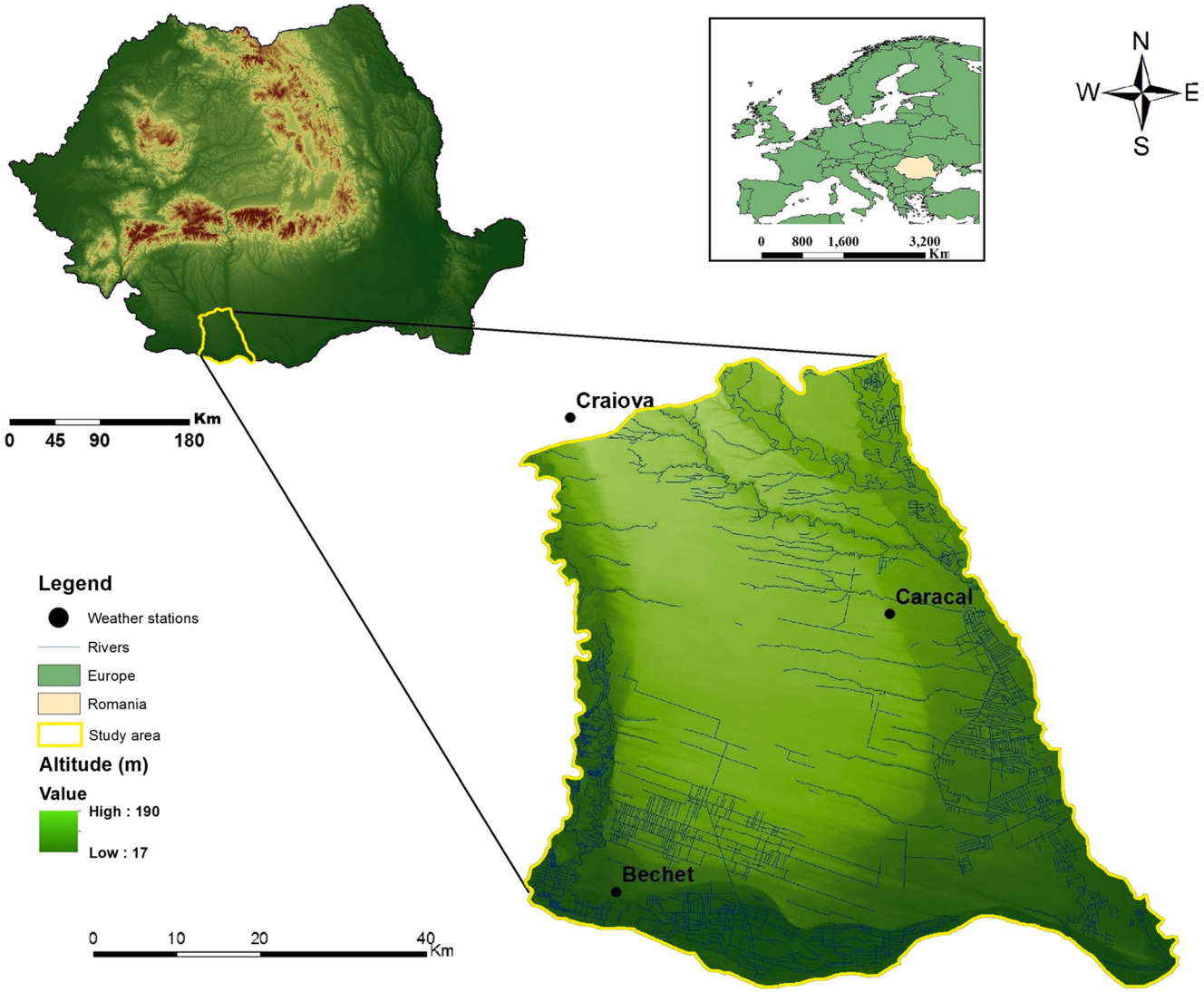


**Fig. 1** Location of study area

Under these circumstances, we considered necessary to investigate the connections between high LST, synoptic conditions, air masses movement, soil type, drought conditions, and natural vegetation and crops land cover area extention.

## 3 Data and methods

Landsat satellite data is one of the most employed satellite products for environmental monitoring studies. The role of remote sensing and GIS to establish the changes detected in agriculture dominated areas has become essential nowadays.

### 3.1 Data used

The study covers a period of 26 years (1986–2011) and the satellite imagery recorded in month of June for 5 years (1986, 1991, 2000, 2007, and 2011) have been used. We have chosen the month of June because it is part of the critical period, when the water requirement of plants is higher than normal. The satellite data has been acquired from U.S. Geological Survey (http//:glovis.usgs.gov). Two satellite scenes have been used to cover the entire territory. They were recorded by the Landsat missions 5 and 7, and they can be identified as WRS 2-Path 184/Row 29 (44.6 N, 23.9 E) and WRS 2-Path 184/Row 30 (43.2 N, 23.4 E), respectively. The details for the satellite data are presented in Table 1.

For the satellite images captured in 2007 and 2011, the scenes cover totally the area, while for scenes collected in 1986, 1991, and 2000, a small part of the area under study is not covered by the data (less than 2 %); for further calculations and analysis for the three study cases, the total area of the region considered has been diminished by the percentage of data uncovered area. Creating a mosaic dataset for the entire study area was not possible for the images collected in 1986,

**Table 1** Landsat imagery data used in this paper

| Sensor | Acquisition date | Acquisition Hour | Cloudiness (%) |
|---|---|---|---|
| TM | 14.06.1986 | 08:29:46 | 0.00 |
| T M | 28.06.1991 | 08:32:24 | 0.00 |
| ETM+ | 28.06.2000 | 09:00:59 | 0.00 |
| TM | 24.06.2007 | 09:03:12 | 0.00 |
| TM | 19.06.2011 | 08:58:37 | 0.00 |

1991, and 2000 because adjacent satellite scenes from the same day were not available.

The soil type map has been provided by Corine Land Cover 2006 project (www.geospatial.org) and daily mean and maximum ground temperatures (*TGmean* and *TGmax*, respectively) recorded in Caracal weather station (WMO code 15469) by National Meteorological Administration (Oltenia Regional Meteorological Center) in Romania.

For synoptic analysis, the Europe's maps with spatial distribution of air pressure at sea level and geopotential at 500 hPa level from Karlsruhe Weather Center e-archive (www.wetterzentrale.de) have been used, for the same day and at the nearest term when the Landsat images have been captured.

For monthly SPEI index calculation, precipitation and daily values of maximum and minimum air temperature recorded in Caracal weather station over a period of 55 years (1961–2015) have been used.

### 3.2 Methods

#### *3.2.1 Satellite data processing*

The algorithm to calculate LST used is based on a procedure developed in few steps by different authors (Markham and Barker 1986; Xie et al. 2012; Imbroane et al. 2014; Herbel et al. 2015). The methodology provides the mathematical operations applied to Landsat satellite imagery by using the ArcMap 10.2 software for map design and ENVI 5.1 software to calculate the LST for the agricultural region located in Southwestern Romania. The Seamless Mosaic tool of ENVI software has been employed to join the two satellite scenes that we used. The general scheme of processing satellite data is presented in Fig. 2.

Step 1. *Conversion of digital number (DN) in spectral radiance.*

Because the thermal radiation received by the satellite is affected by the atmosphere, an accurate temperature cannot be obtained directly from the sensors. The TM and ETM+ sensors of Landsat missions store the spectral response of objects in the thermal infrared region (10.4–12.5 μm for band 6) as digital numbers (DNs) with values ranging from 0 to 255 and a radiometric resolution of eight bits. Therefore, the calibrated digital numbers have to be converted to radiance values. In this model, we used the equation developed by Markham and Barker (1986) to calculate the spectral radiance (1).

$$L_\lambda = L_{\min(\lambda)} + \left(L_{\max(\lambda)} - L_{\min(\lambda)}\right) Q_{\mathrm{dn}} / Q_{\max} \quad (1)$$

where $L_\lambda$ is the spectral radiance for wavelength λ; $Q_{\mathrm{dn}}$ is the gray level of each pixel; $Q_{\max}$ is the maximum numerical value of the pixel; $L_{\max(\lambda)}$ and $L_{\min(\lambda)}$, respectively, are the minimum and maximum spectral radiance for $Q_{\mathrm{dn}} = 0$ and $Q_{\mathrm{dn}} = 255$. The $L_{\max(\lambda)}$ and $L_{\min(\lambda)}$ values vary for each Landsat scene. These specific values can be found in the metadata file downloaded with the images.

Step 2. *Conversion of radiance to temperature*

The next step is to convert the spectral radiance into satellite brightness temperature. We used a simplified procedure to compute the blackbody temperature adapted for Landsat satellites imagery by Markham and Barker (1986). Assuming surface emissivity being equal to that of the black body, the formula for conversion is similar to Plank's equation calculated based on two free parameters (Xie et al. 2012), as in (2):

$$T_b = \frac{K_2}{\ln(K_1/L_\lambda + 1)} \quad (2)$$

where $T_b$ is the blackbody temperature (in Kelvin); $L_\lambda$ is the spectral radiance derived above; and $K_1$ and $K_2$ are the calibration constants (given by the sensors producer):

i. for Landsat 5: $K_1 = 607.76$ watts/(meter squared × ster × μm) and $K_2 = 1260.56$ K
ii. for Landsat 7: $K_1 = 666.09$ watts/(meter squared ×ster × μm) and $K_2 = 1282.71$ K

Step 3. *Extraction of vegetation coverage*

We have calculated NDVI in order to determine the raster emissivity and after that to determine the LST. The reflectance in red and near infra-red has been combined to get the relationship between the radiometric response of the crops and their vegetative structure. Thus, NDVI has been calculated as in (3):

$$\mathrm{NDVI} = \frac{B4 - B3}{B4 + B3} \quad (3)$$

where *NDVI* is the normalized difference vegetation index; *B3* is the band 3 (red) of Landsat TM (for 1986, 1991, 2007, and 2011) and ETM+ (2000); and *B4* is the band 4 (near infra-red) of Landsat TM (for 1986, 1991, 2007, and 2011) and ETM+ (2000).

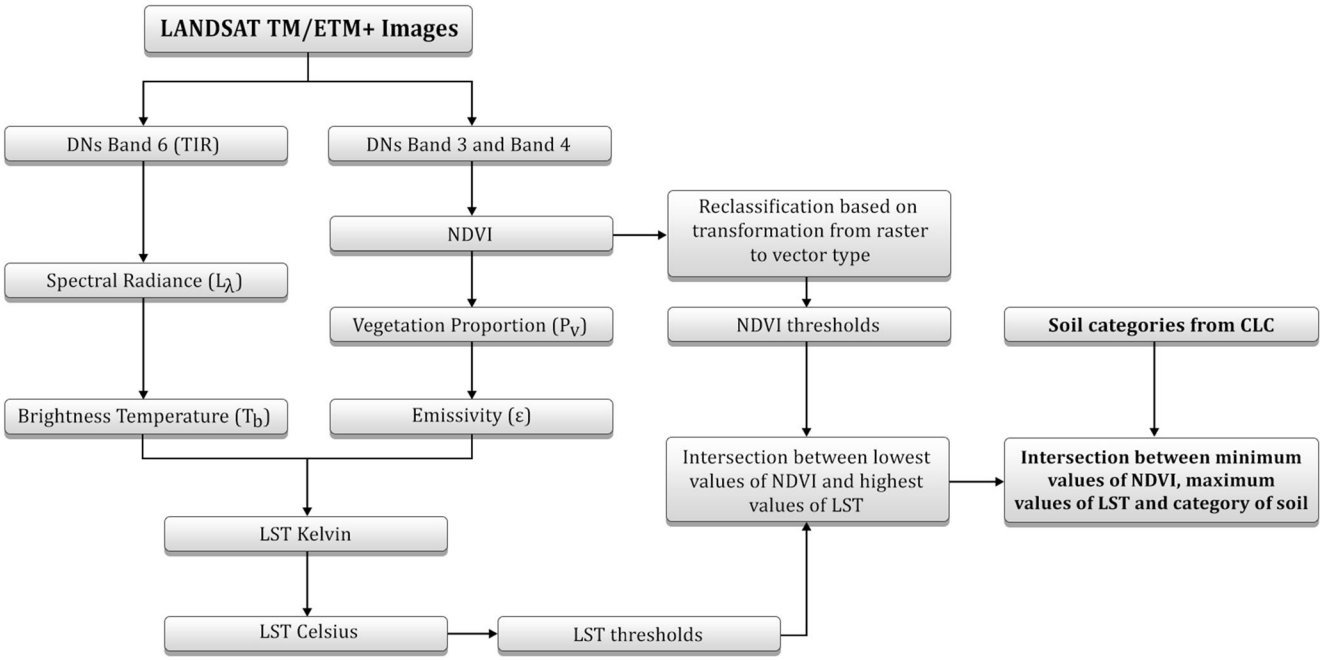


**Fig. 2** Algorithm for satellite data processing

Based on this procedure, raster data ranging from −1 to 1 are issued. Positive values indicate areas with vegetation, while negative values indicate areas without vegetation such as bare soil, human settlements, or water. NDVI also provides information about the health of vegetation.

Step 4. *Calculation of the proportion of vegetation*

Furthermore, based on NDVI values, the method proposed by Carlson and Ripley (1997) has been employed to calculate the proportion of vegetation for every pixel in the study area, as in (4).

$$Pv = [(\mathrm{NDVI}-\mathrm{NDVI}_{\min})/(\mathrm{NDVI}_{\max}-\mathrm{NDVI}_{\min})]^2 \quad (4)$$

where $Pv$ is the vegetation proportion; $NDVI_{\min}$ is the NDVI values for bare soil pixels; and $NDVI_{\max}$ is the NDVI values for fully vegetated pixels.

Step 5. *Calculation of the land surface emissivity (LSE)*

The calculation of land surface emissivity (LSE) is an important step to get LST, and the final emissivity raster has been obtained according to procedure developed by Sobrino et al. (2004) (5):

$$\varepsilon = 0.004Pv + 0.986 \quad (5)$$

where $\varepsilon$ is the LSE values of the pixel and $Pv$ is the vegetation proportion from (4).

Step 6. *Calculation of LST*

The LST in the study area was then computed by performing emissivity corrections on the brightness temperature obtained from (2). The method used for scaling the black-body temperature was the one developed by Artis and Carnahan (1982) and recently used by Feizizadeh and Blaschke (2013), as shown in (6).

$$LST = \frac{T_b}{1 + (\lambda T_b/\rho)\ln\varepsilon} \quad (6)$$

where $T_b$ is the black body temperature; P is the $h \times c/\sigma$ ($1.438 \times 10^{-2}$mK); $H$ is the Plank's constant ($6.626 \times 10^{-34}$ J s); $\Sigma$ is the Boltzman's constant ($1.38 \times 10^{23}$ J/K); $c$ is the light velocity ($2.998 \times 10^{8}$ m/s); λ is the wavelength of emitted radiance (11.4 μm for Landsat TM and ETM+ bands); and ε is the LSE.

Step 7. *LST conversion from Kelvin to Celsius degrees*

Since the LST value obtained in (6) is given in Kelvin, the final step for LST retrieval is to convert LST from Kelvin to Celsius degrees (7).

$$LST_C = LST - 273.15 \quad (7)$$

where $LST_C$ is the temperature in °C and $LST$ is the temperature in K.

For further analysis in the "Results and Discussions" section as well as in the "Conclusions" section, the LST will be given in Celsius, although the *LST* acronym will be used instead of $LST_C$.

Step 8. *Reclassification based on NDVI, LST values, and soil types*

After obtaining the raster results for NDVI, LST, and soil types, reclassifications have been performed for each parameter.

Thus, for NDVI, three classes have been established:

i. High density vegetation (NDVI values from 0.6 to 1.0);
ii. Low density vegetation (NDVI values from −0.5 to 0.5);
iii. Lack of vegetation class (NDVI values from −1.0 to −0.6), which was considered the most appropriate to be used for this study.

The LST values have been divided into two classes:

i. High-temperature class (LST≥ 40.0 °C);
ii. Low-temperature class (LST < 40.0 °C).

The soil types have also been reclassified in four main classes:

i. Sandy soils;
ii. Brown soils;
iii. Chernozems;
iv. Other soil types

On the maps, we identified a class of waterbodies.

For further analysis, one class has been retained both for NDVI and LST (lack of vegetation class and high-temperature class, respectively), as well as all soil classes.

Step 9. *Intersection of polygons derived from NDVI, LST, and soil categories reclassification*

A transformation from raster to vector files was followed in the algorithm, in order to calculate the area of polygons with high-temperature and lack of vegetation for different soil class. First, the intersection of high-temperature and lack of vegetation polygons has been performed and further on the resulting polygons have been intersected by those resulted from soil reclassification.

### *3.2.2 Air particle backward trajectories*

After getting the remote sensing results, we have performed a specific analysis based on the origin of the air particles that caused the atmospheric conditions in the five study cases considered for this paper.

To detect the source areas of the air masses, the atmospheric backward trajectories of the air particles have been simulated by employing the online version of HYSPLIT model Real-time Environmental Application and Display sYstem (READY), developed by National Oceanic and Atmospheric Administration (NOAA) (Rolph 2011, 2016; Draxler and Rolph 2011; Stein et al. 2015).

We have used, for this paper, backward trajectories detected at three levels, from near-ground level (200 m above ground level—AGL) up to mid-troposphere (2000 and 5000 m AGL, respectively). These levels have been chosen in order to allow the identification of possible different source-region of air masses and the existence of different air masses in low and middle troposphere, respectively, over the considered region.

The backward trajectories have been run for 72 h, ending at 09.00 UTC (i.e., 12.00 Romanian Summer Time—RST). Before choosing the time-span to run the trajectories, we have performed few trials, but finally we have retained the time-span of 72 h before the ending point. We have found it long enough to allow the identification of the air masses origin, especially in higher altitude where the velocity of the air flow is much higher compared to that of near-ground level.

The vertical transport has been modeled at every 6 h, by employing the vertical velocity option of HYSPLIT application, and thus five maps have been derived, with source point in Caracal city, Romania (44.10 N, 24.34 E), located approximately in the middle of the region. The ending time is very close to the satellite image capture and thus our analysis could provide useful information on the air masses generating the highest LST in the considered region. The changes in the air parcel height, along its trajectory, have also been investigated. This type of analysis has provided useful information that helped to explain some temperature variation.

The meteorological input for the trajectory model has been the reanalysis dataset, freely provided by NCEP/NCAR Reanalysis (available at http://rda.ucar.edu/). HYSPLIT application uses archived three-dimensional meteorological fields generated from observations and short-term forecasts (Stein et al. 2015).

### *3.2.3 Correlation methods*

The scaterogram analysis indicates that the most appropriate correlation for the data available for this paper is a linear one. Under these circumstances and in order to get more accurate results, we have decided to use more than one correlation type for analysis of correlation between different pairs of variables considered: area without vegetation and area with LST ≥ 40.0 °C; LST and ground level temperature, *TGmean*, and *TGmax)*. Thus, Pearson product moment

correlation coefficient, logarithmic, and quadratic correlation coefficients have been calculated. All of them are methods of correlation between two variables ($x$ and $y$) largely used in climatic and environmental studies (Dada et al. 2016; Trigo et al. 2016; Ma et al. 2016; Pan 2016; Van de Griend and Owe 1993; Carabaño et al. 2016; Nasri et al. 2016).

The data have been processed by using SPSS statistical software, version 19.0.0.

#### *3.2.4 Drought conditions assessment method*

The measure of drought and wet conditions is a complex issue, but the wide fields of activities affected and the different scales they operate on make it difficult to develop both a definition to describe and an index to measure them. Some of the indices developed so far consider that the drought is cumulative, so the intensity of drought during the current period is dependent on the current precipitation plus the cumulative precipitation of the previous period. When applied to longer periods of time, this function denotes dry and wet periods and shows some other climate characteristics. This approach has been implemented in many drought indices (standard precipitation index, surplus and deficit of precipitation, standard precipitation and evapotranspiration index, etc.) for different time scales (1 month, 3 months, 6 months, 12 months, etc.), as the information obtained could be useful in different domains (Radinović and Ćurić 2009).

In order to assess the water availability conditions of the area in the period when the Landsat images were collected (month of June), we used the Standardized Precipitation and Evapotranspiration Index (SPEI), developed by Vicente-Serrano et al. (2010), for three time steps (1, 3, and 6 months) calculated for Caracal weather station.

## 4 Results and discussion

Solar radiation is the most important factor generating high temperature followed by air circulation as the secondary. Combined with lack of precipitation, high temperature results in dryness or severe drought episodes. Both atmospherical and pedological droughts have a negative impact on plants transpiration and photosynthesis. The stressing environmental factors influence plants causing physiological adjustments and changes in phenology. Water scarcity in the absence of irrigation results in wilted plants, and this is a more and more frequent situation in the last two decades in the area under study. In general, plants density decreases when more or less severe drought events occur, especially generated by dramatically decreasing rainfall and increasing temperature.

At the beginning of the period considered, an intensive agriculture with cereals crops, fruit trees, and vineyard (the last two were cultivated especially on sandy soils) developed based on rational use of fertilizers and by supplementing the water deficit through an irrigation system.

Currently, the lack of irrigation system has made from the area under research an improper environment for such intensive agriculture. In the next sub-chapters, five situations will be analyzed in order to establish the relationships among LST, air circulation, (lack of) vegetation, and soil type.

### 4.1 Correlation between measured and estimated ground temperature

The Romanian national network of weather stations is not dense enough to cover the necessity of information, especially in agriculture fields. Thus, the first analysis we performed in terms of correlation was to find the relationship between ground temperature measured in a weather station (Caracal) and the LST derived from satellite images for the pixel where the weather station is located. Caracal is the only weather stations in the region with recordings of soil temperature available (Table 2). Under these circumstances, we considered useful to calculate the correlation coefficient between temperature derived from satellite images and ground level measured temperature in order to assess the potential of using satellite images derived temperature for the areas without direct observations.

The best correlation was found between LST and *TGmax* (0.788 for all coefficients); for *TGmean*, the correlation was much lower, between 0.453 and 0.709. One can see that correlation values got for measured and estimated ground temperature are similar in case of all coefficients for *TGmax*, while for correlation between estimated LST and *TGmean*, the quadratic function showed a considerably higher value than Pearson and logarithmic, respectively (Table 3). Also, it should be mentioned that correlation between LST and *TGmean* is somehow irrelevant, since the mean temperature is calculated from four values recorded over a 24-h period, while LST is a momentum temperature.

### 4.2 Correlation between high LST and low NDVI areas

High temperature and low precipitation amounts in summer months have a great impact on vegetation, due to frequent drought events with different intensity, which are specific in the area under the influence of Mediterranean climate conditions.

The high temperature of this period can become dangerous to plants growth when over passing some specific values. Thus, when the temperature exceeds 35.0 °C, the intensity of photosynthesis drops close to lower limit, while in case of temperature higher than 45.0 °C, the photosynthesis process stops. Under these circumstances, an imbalance appears between absorption and transpiration processes followed by

**Table 2** LST and areas without vegetation detected from satellite image and ground temperature recorded in Caracal Weather Station

| Date | Time of satellite image | LST (°C) | Area without vegetation (%) | Area with LST ≥ 40.0 °C (%) | Interval of measurement | Ground temperature in Caracal (°C) | |
|---|---|---|---|---|---|---|---|
| | | | | | | TGmean | TGmax |
| 06/14/1986 | 08:29:46 | 25.9 | 15.60 | 9.94 | 00:06–18:00 | 26.0 | 38.6 |
| 06/28/1991 | 08:32:24 | 31.1 | 40.60 | 30.32 | 00:06–18:00 | 33.1 | 56.0 |
| 06/28/2000 | 09:00:59 | 42.4 | 71.45 | 59.65 | 00:06–18:00 | 30.3 | 61.0 |
| 06/24/2007 | 09:03:12 | 33.6 | 33.03 | 17.20 | 00:06–18:00 | 28.9 | 42.2 |
| 06/19/2011 | 08:58:37 | 27.8 | 11.21 | 8.58 | 00:06–18:00 | 28.3 | 42.3 |

The time is given in UTC

leaves dehydration and chlorophyll decomposition (Martin 1968).

The second correlation in this study has been performed between high LST areas and surfaces without vegetation (low NDVI class) (Table 3).

A strong correlation (0.981–0.987) has been found between the total area with LST equal or higher than 40 °C and the total area uncovered by vegetation when considered all study cases: the area with lack of vegetation derived from NDVI values increases with the increase of the area with high-temperature class detected based on LST values (Table 3).

### 4.3 Analysis of study cases

#### *4.3.1 June 1986*

The first valid satellite image captured for the area under study is from 14th of June 1986. The air circulation detected based on HYSPLIT model indicated an east-northeast advection in the 72 h before the moment of the satellite image capture (Fig. 3a), but based on the synoptic map analysis (Fig. 4a), the advection of the air mass occurred on the front branch of a warm high-altitude ridge originating in Atlantic Ocean and crossing Western and Central Europe at mid-latitude. At sea level, an extended anticyclone was active all over the Europe. Under these conditions, both in higher altitude and near the ground level, the trajectories are similar. The "original" oceanic air became drier and warmer while crossing the whole continent until reaching Eastern Europe and generated high temperature at ground level in the area under study.

The satellite image processing revealed the area with LST equal to or higher than 40.0 °C covering almost 10 % of the total surface in the considered region (Fig. 5a, b).

Furthermore, we identified the impact of such high temperatures on vegetation cover. Analysis based on satellite image indicated an area without vegetation of 15 % from the whole considered surface (Table 2 and Fig. 5c, d). However, the dense vegetation cover, compared to other situations that are to be presented in the following sub-chapters, is supposed to be determined by the presence of irrigation system that was in action at that time, as well as by near normal SPEI value for the month of June 1986, for all time steps (Table 4). Another anthropogenic factor to be mentioned is that in the period under discussion, all the fields were cultivated as they were property of the state and an intensive agriculture development was the main aim of the decision makers of that time.

When overlap the soil types map, it has to be emphasized that most of surfaces with high LST and lack of vegetation are located in southwestern part of the region, where sandy soils are dominant (Fig. 5e, f). They are followed by classes of "other types" soils and chernozems (Table 5).

**Table 3** Correlation values calculated between LST and different parameters in the area

| Correlation value between: Correlation type | LST[a] in the pixel of Caracal weather station and *TGmax* | LST in the pixel of Caracal weather station and *TGmean* | Area[b] without vegetation and area with LST ≥ 40.0 °C |
|---|---|---|---|
| Pearson | 0.788 | 0.453 | 0.981 |
| Logarithmic | 0.788 | 0.494 | 0.984 |
| Quadratic | 0.788 | 0.709 | 0.987 |

[a] Both LST and mean/maximum ground temperature are given in °C

[b] The areas are given in % of the total area of the region

#### *4.3.2 June 1991*

The second valid satellite image was captured on the 28th of June 1991.

The backward trajectories of air particles analysis revealed that in the previous 3 days, in the higher levels, a western air flux was dominant at higher levels considered (2000 and 5000 m) (Fig. 3b). In the middle troposphere, the air particles crossed the Northern Iberian Peninsula, Northern Mediterranean and Adriatic Seas, Northern Italy and Balkan Peninsula. Up to 200 m, the air mass was characterized by a slow velocity which allowed a radiative warming. Under the

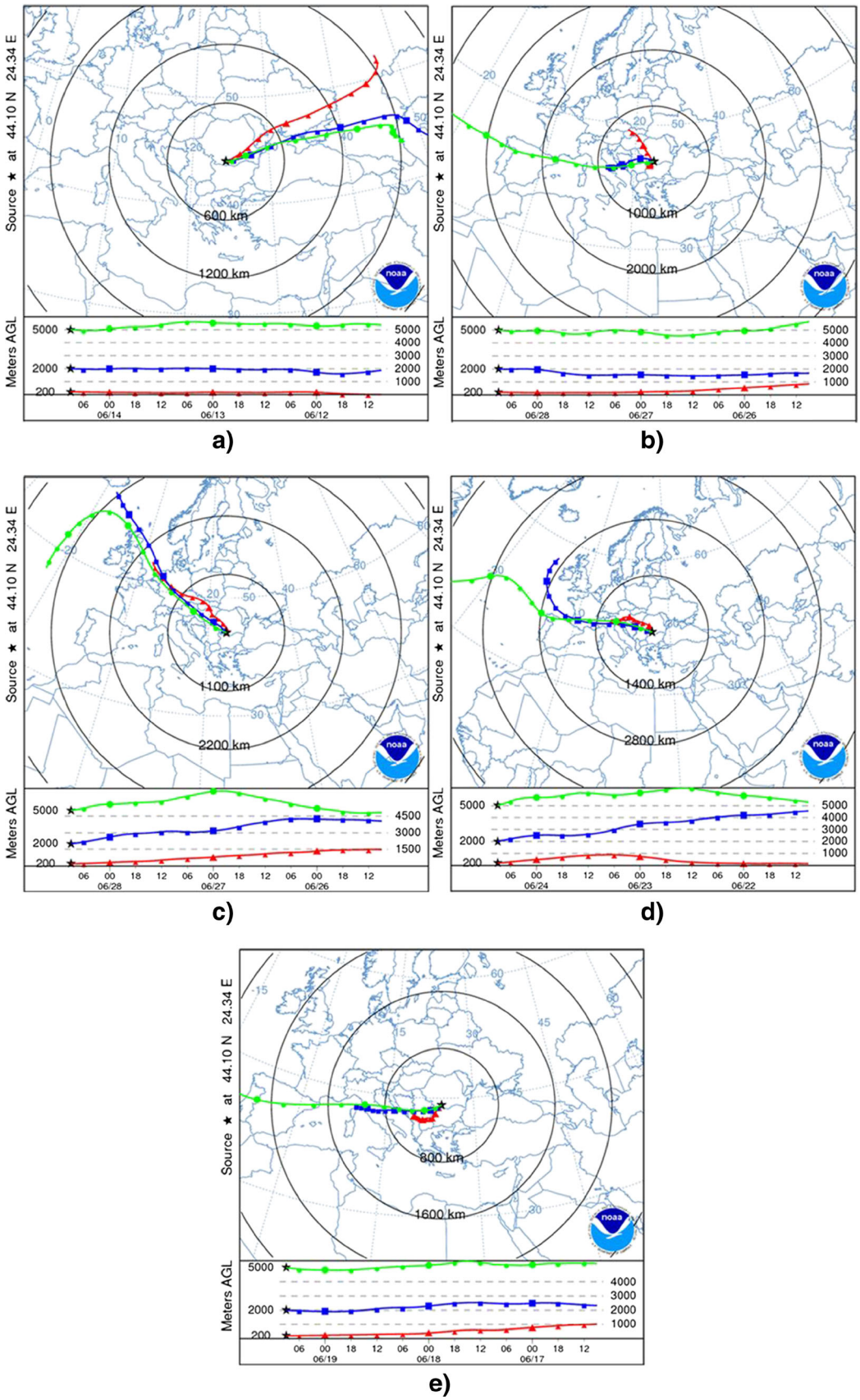


**Fig. 3** Backward trajectories of air particles for the interval of 72 h before satellite image capture time, based on NOAA HYSPLIT Model

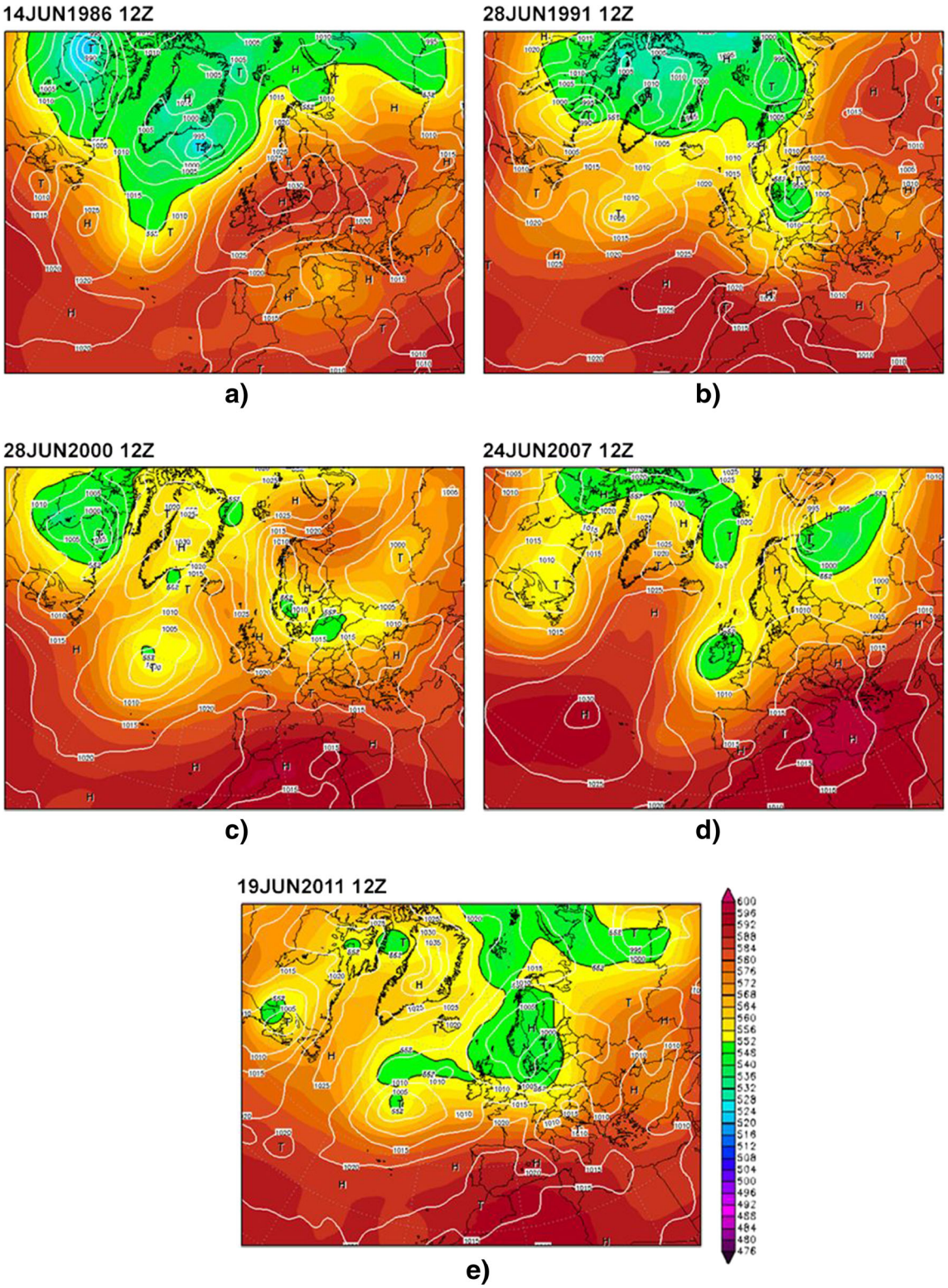


**Fig. 4** Sea level air pressure and geopotential at 500 hPa level over Europe

influence of a small tropical ridge at 500 hPa level (572–576 damg), blocked in its movement northward by a cut-off nucleus extended over Northern Germany, Western Poland and Denmark (Fig. 4b), the air temperature continuously increased in the 3 days before the satellite image capture, slowly in the upper levels, and more pronounced at near ground level. At sea level, below normal air pressure was dominant over the entire continent. The data recorded at

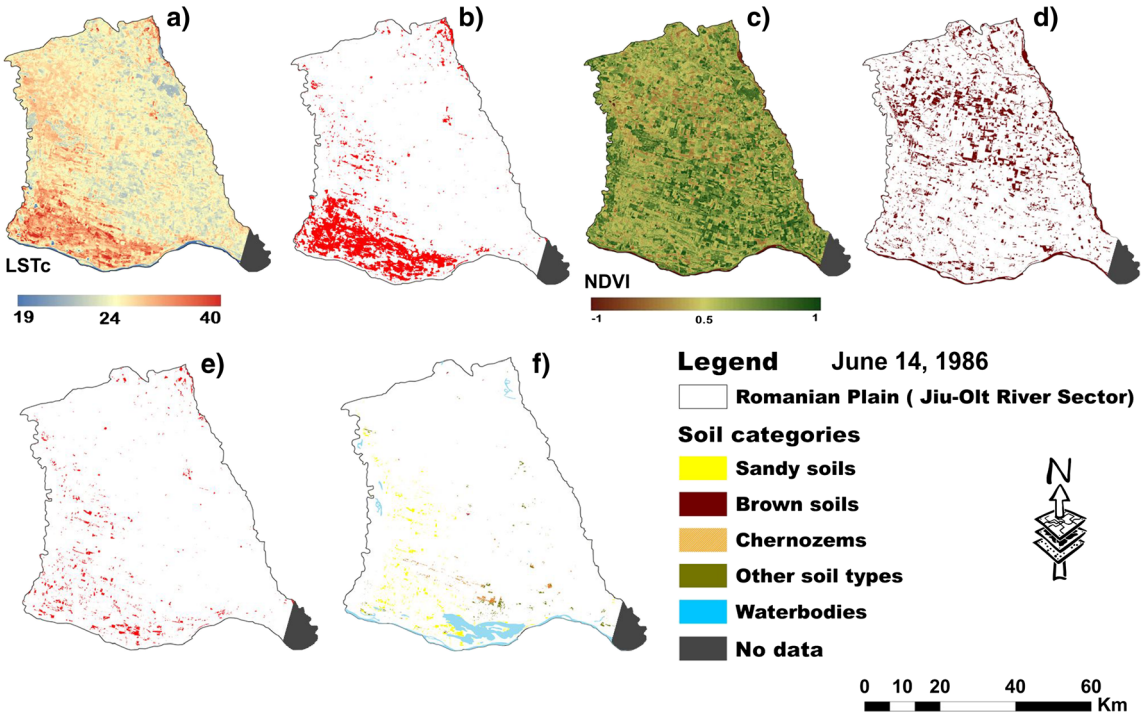


**Fig. 5** LST, NDVI, and soil types on the 14th of June 1986 (**a** LST; **b** polygons with LST ≥ 40.0 °C (%); **c** NDVI; **d** polygons with lack of vegetation; **e** polygons with intersection between lack of vegetation and LST ≥ 40.0 °C; **f** polygons with intersection of (**e**) and soil categories)

Caracal weather station located in the area under study indicated a mean ground temperature of the day higher than 33.0 °C, while the maximum value reached 56.0 °C (Table 2). The monthly SPEI value was near normal for one-month time step.

Under these circumstances, the area with LST equal to or higher than 40.0 °C covered more than 30 % of the total region (Fig. 6a, b), and the impact of high temperature recorded in the air and soil on vegetation was much more consistent compared to the situation in June 1986: the area without vegetation was even larger than the one with high LST and reached more than 40 % of the entire region (Table 2, Fig. 6c, d).

In order to identify the most prone soil types to high LST and lack of vegetation, we have overlapped the polygons without vegetation, high LST polygons (Fig. 6e), and soil types polygons. Finally, we found that the most exposed soil type to high LST and lack of vegetation are the sandy soils (more than 27 %), followed by brown soils (more than 14 %), and chernozems (more than 11 %) (Fig. 6f).

### *4.3.3 June 2000*

The third valid satellite image for the month of June was captured on the 28th of June 2000.

The backward trajectories analysis revealed that in the 3 days before the time of the satellite image capture, an air mass coming through a ridge extended over North Atlantic from Azores High, was identified in higher layers (2000 and 5000 m AGL, respectively) (Figs. 3c and 4c). In the three previous days, the air masses at lower level (200 m AGL), characterized by a considerably slower velocity toward south-east, warmed significantly under clear sky and high solar

**Table 4** SPEI values and conditions calculated for Caracal weather station for three time steps (classes have been assimilated to conditions given by Abdullah, 2014)

| Year | One-month time step | | Three-months time step | | Six-months time step | |
|---|---|---|---|---|---|---|
| | Value | Class | Value | Class | Value | Class |
| 1986 | 0.88 | NN | −0.9 | NN | 0.49 | NN |
| 1991 | 0.07 | NN | 1.6 | SW | 0.89 | NN |
| 2000 | −1.77 | SD | −2.1 | ED | −1.90 | SD |
| 2007 | −0.61 | NN | −1.4 | MD | −1.33 | MD |
| 2011 | 0.69 | NN | 0.20 | NN | 0.29 | NN |

*NN* near normal, *MD* moderately drought, *SD* severe drought, *ED* extremely drought, *MW* moderately wet, *SW* severe wet

**Table 5** Areas of polygons with LST equal to or higher than 40.0 °C, low vegetation cover, and soil types (%)

| Soil type | Area covered (%) | 1986 | 1991 | 2000 | 2007 | 2011 |
|---|---|---|---|---|---|---|
| Sandy soils | 51.8 | 4.1 | 27.2 | 54.2 | 22.0 | 5.5 |
| Brown soils | 18.5 | 0.1 | 14.2 | 65.9 | 2.7 | 0.1 |
| Chernozems | 15.2 | 1.7 | 11.3 | 49.6 | 19.2 | 1.7 |
| Other soil types | 11.4 | 2.1 | 5.4 | 4.7 | 3.8 | 1.4 |
| Waterbodies | 3.1 | 2.0 | 10.8 | 18.4 | 2.8 | 2.0 |

radiation amount conditions over Central and South-Eastern Europe which was dominated by a weak anticyclone (Fig. 4c). Therefore, at the moment when the air mass arrived at the final point it was warmer compared to its origin point.

The situation in June 2000 seems to be the most dramatic one among all considered for this study. Recognized as one of the warmest and driest years of the last century (Marinică 2006), the maximum air temperature recorded in the south-west of the region was 39.8 °C, the rainfall was about 20 mm for the entire month of June (representing less than 25 % of the mean multiannual amount), and the mean monthly relative humidity was about 59 % (Roşca 2012), resulting in SPEI values indicating severe drought conditions for 1- and 6-month time steps, while extremely drought conditions were calculated for the 3-month time step (Table 4). The maximum soil temperature recorded in Caracal weather station for 28th of June was 61.0 °C (Table 2), which is supposed to have been recorded few hours later, in the afternoon, after satellite image capture. The LST derived from the satellite image rose to more than 42.0 °C, at 9:00 am, in the pixel where the weather station is located. Those conditions were specific to a severe drought event, which began in May and lasted for few months afterwards. Under these circumstances, by the end of June, the total area with LST equal or higher than 40.0 °C reached almost 60 % (Fig. 7a, b, Table 2), while the lack of vegetation area extended over more than 71 % of the region (Fig. 7c, d, Table 2).

When high LST values, lack of vegetation and soil type polygons were overlapped (Fig. 7e, f), we found that about half of areas or even more in case of some main soil categories was characterized by lack of vegetation and high LST. The most affected was vegetation on brown soils, followed by those on sandy soils and chernozems (Table 5). It worth mention that the disastrous situation may be due also to lack of irrigation in the region, since at that period the irrigation system was completely damaged and out of work.

### *4.3.4 June 2007*

For the June 2007 case study, all trajectories indicated a western-southwestern air flux, with more rapid high trajectories (2000 and 5000 m AGL) crossing the European continent from the Atlantic Ocean eastward to the region considered, while at near-ground level, the air particle had a slower movement (original location in Northern Italy) (Fig. 3d). Synoptic map analysis reveals a northward moving ridge originated in Northern Africa

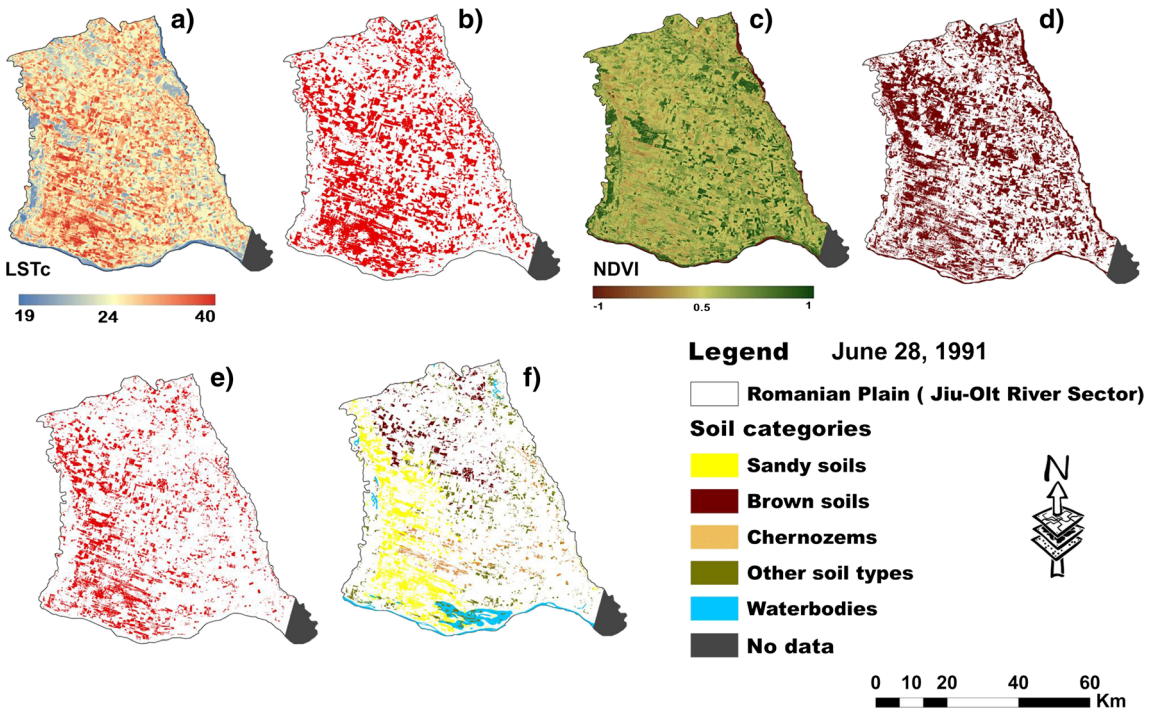


**Fig. 6** LST, NDVI, and soil types on the 28th of June 1991 (**a** LST; **b** polygons with LST ≥ 40.0 °C (%); **c** NDVI; **d** polygons with lack of vegetation; **e** polygons with intersection between lack of vegetation and LST ≥ 40.0 °C; **f** polygons with intersection of (**e**) and soil categories)

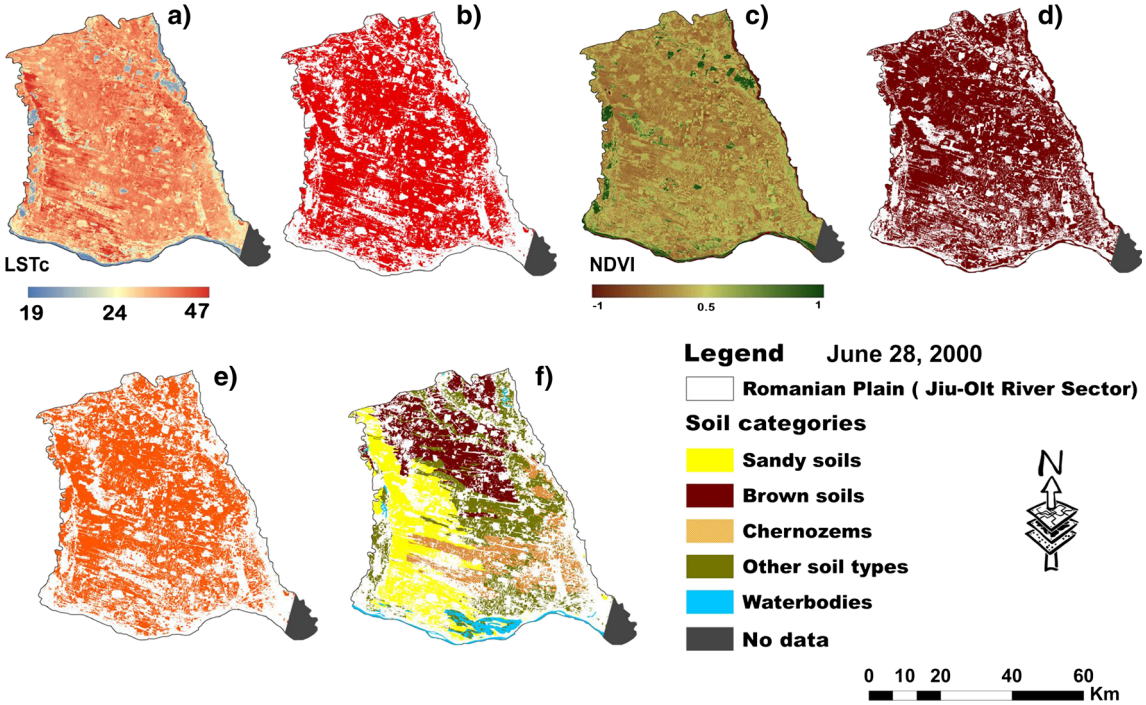


**Fig. 7** LST, NDVI, and soil types on the 28th of June 2000 (**a** LST; **b** polygons with LST ≥ 40.0 °C (%); **c** NDVI; **d** polygons with lack of vegetation; **e** polygons with intersection between lack of vegetation and LST ≥ 40.0 °C; **f** polygons with intersection of (**e**) and soil categories)

and Southern Mediterranean in mid-troposphere, while at sea level, a weak anticyclone extended over the most part of Southern and Central Europe was dominant (Fig. 4d).

From agricultural point of view, weather conditions in spring of the year 2007 were critical, due to lack of precipitation recorded in the two weather stations in the area (Bechet and Caracal), during the germination period of the crops, especially in April. The combined impact of low precipitation and high temperature on crops continued in May and June, when SPEI index conditions indicated moderate drought for 3- and 6-month time steps, respectively (Table 4). Under those conditions in the considered region, low values of NDVI were recorded as well as high ground and air temperatures by the end of June. Thus, from the entire area, polygons with LST equal or higher than 40.0 °C covered more than 17 % of the area (Fig. 8a, b). It worth mention that this situation may be also explained by the presence of a heat wave occurred over the period 18–27.06.2007 in Southwestern Romania, with the highest temperature in the air of 38.6 °C (Croitoru 2014). The polygons without vegetation covered more than 33 % of the region (Fig. 8c, d). Area with LST equal or higher than 40.0 °C and without vegetation covered 22 % of the sandy soils area and 19.2 % of the chernozems area (Fig.8e, f, Table 5).

*4.3.5 Analysis of situation on June 2011*

The general circulation in the middle troposphere before 19th of June 2011 was quite similar to that recorded for June 2007, having its origin in the Atlantic Ocean and was characterized by a general trajectory eastward (Fig. 3e). The air mass near the ground, present on the 19th of June 2011 in the area of interest, was affected in the three previous days by a weak counter-clockwise rotation from the Adriatic Sea shoreline. This movement could be influenced by the back branch of a ridge developed over Eastern Europe in mid-troposphere and by the weak cyclone developed behind it at the ground level (Fig. 4e).

The variability of air temperature for each month of June considered in this study depends especially on the circulation fluxes. Due to western advection in middle troposphere bringing important precipitation, the month of June 2011 was characterized as having almost optimum weather conditions for crops growth, proved by near normal conditions given by SPEI index (Table 4). Few rainy days associated to the passage of a warm front occurred before the day when the satellite image was taken.

Under these circumstances, the area covered by high LST was much smaller (less than 9 %) compared to previous situations (Fig. 9a, b), especially due to evapotranspiration process which considerably diminished the LST values. At the same time, the area without vegetation was the smallest among all study cases considered and extended over less than 12 % of the entire region (Fig. 9c, d). The highest values of LST were specific in the south of region where the sandy soils that favored rapid infiltration of rainfall water are dominant (Fig. 9e, f).

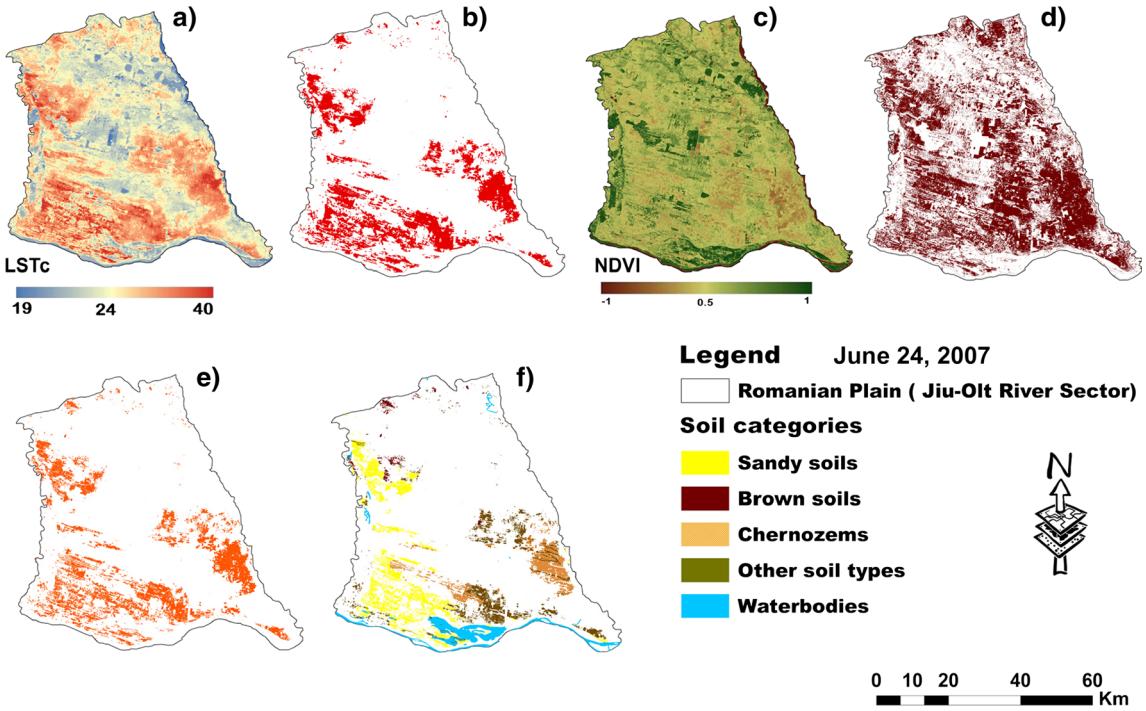


**Fig. 8** LST, NDVI, and soil types on the 24th of June 2007 (**a** LST; **b** polygons with LST ≥ 40.0 °C (%); **c** NDVI; d. polygons with lack of vegetation; **e** polygons with intersection between lack of vegetation and LST ≥ 40.0 °C; **f** polygons with intersection of (**e**) and soil categories)

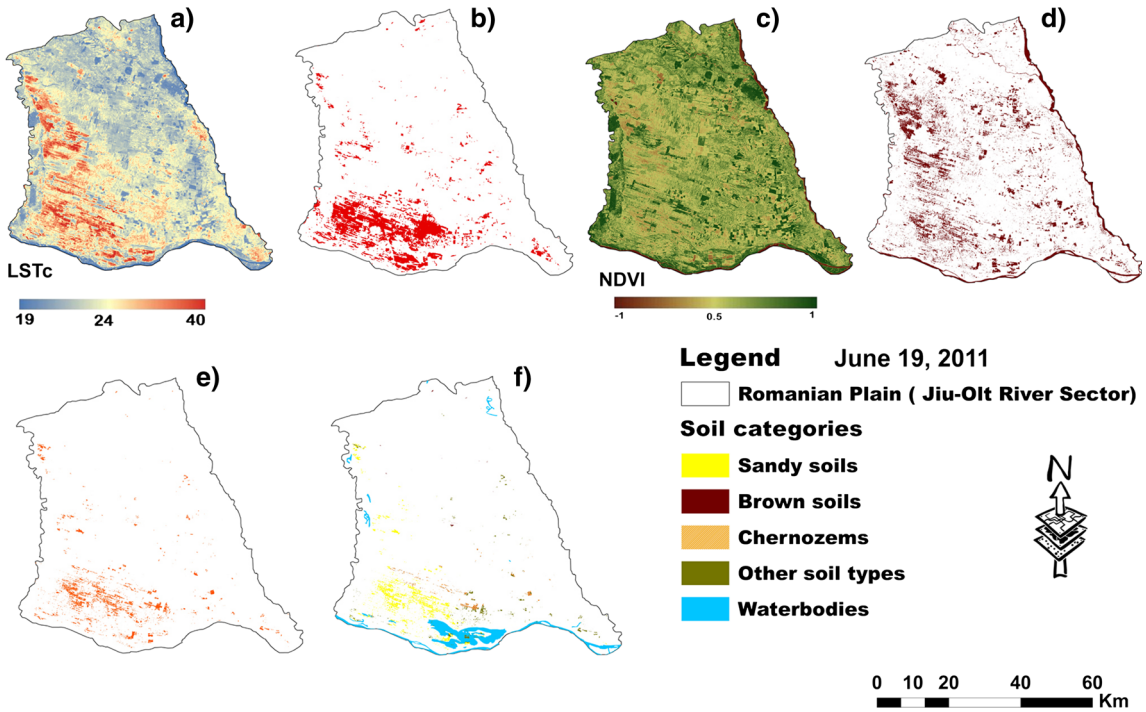


**Fig. 9** LST, NDVI, and soil types on the 19th of June 2011 (**a** LST; **b** polygons with LST ≥ 40.0 °C (%); **c** NDVI; **d** polygons with lack of vegetation; **e** polygons with intersection between lack of vegetation and LST ≥ 40.0 °C; **f** polygons with intersection of (**e**) and soil categories)

## 5 Conclusions

Satellite images recorded in the month of June, but in different years along a 26-year period, revealed that climatic and non-climatic factors definitely influence LST and vegetation cover. Among the climatic factors, solar radiation is the most important one, which in anticyclone conditions developed at ground level under ridges in mid-troposphere, leads to maximum ground temperature values, both measured and estimated from satellite images.

The air mass trajectories analysis is more relevant when performed together with synoptic analysis, because they can give more useful information on extremely hot spells occurring conditions. Soil types and changes in the land use, some of them due the geo-politic context or socioeconomic conditions (the irrigation system destruction, land abandonment, and low income in the region), are the most important non-climatic factors identified.

Transition from an intensive agriculture coordinated exclusively by state institutions to the situation coordinated by individual owners with small properties could partially explain the results of NDVI values and distribution over the period 1986–2011.

As a general overview of the study cases, we can conclude that the impact of LST equal or higher than 40 °C on vegetation cover, detected by using NDVI, is very high as we found a very strong correlation between areas with lack of vegetation and those with high LST.

Also, we identified, for the study region, the sandy soils as the most prone soil types to high LST and lack of vegetation cover, followed by the chernozems and brown soils. It is remarkable that most of the areas with high LST and lack of vegetation are located on sandy soils in southwestern part of the region.

It worth mentioning that the region may be affected by severe drought events, as that in 2000, when more than 70 % of the total surface was affected by lack of vegetation. Under these circumstances, local and central authorities should adopt the most appropriate measures in order to avoid the negative impact of such events.

**Acknowledgments** This research was developed under the framework of the project *Extreme weather events related to air temperature and precipitation in Romania*, project code PN-II-RU-TE-2014-4-0736, funded by the Executive Unit for Financing Higher Education, Research, Development, and Innovation (UEFISCDI) in Romania.

The authors acknowledge the USGS for freely provided LANDSAT imagery, and Oltenia Regional Meteorological Center for ground temperature data.

Also, special acknowledgements are for the two anonymous reviewers for their useful comments and suggestions which helped us to improve the quality of this paper.

## References

Abdullah HM (2014), Standardized precipitation evapotranspiration index (SPEI) based drought assessment in Bangladesh. Proceedings of 5th International Conference on Environmental Aspects of Bangladesh [ICEAB 2014]. Paper ID 23:40–42

Adame JA, Valentí–Pía MD, Gil-Ojeda M (2015) Impact evaluation of potential volcanic plumes over Spain. Atmos Res 160:39–49. doi:10.1016/j.atmosres.2015.03.002

Amiri R, Weng Q, Alimohammad A, Alavipanah SK (2009) Spatial–temporal dynamics of land surface temperature in relation to fractional vegetation cover and land use/cover in the Tabriz urban area, Iran. Remote Sens Environ 113:2606–2617. doi:10.1016/j.rse.2009.07.021

Anderson MC, Norman JM, Mecikalski JR, Torn RD, Kustas WP, Basara JB (2004) A multi-scale remote sensing model for disaggregating regional fluxes to micrometeorological scales. J Hydrometeorol 5:343–363. doi:10.1175/1525-7541(2004)005<0343:AMRSMF>2.0.CO;2

Artis DA, Carnahan WH (1982) Survey of emissivity in thermography of urban areas. Remote Sens Environ 90:313–329. doi:10.1016/0034-4257(82)90043-8

Bogawski P, Bednorz E (2016) Atmospheric conditions controlling extreme summertime evapotranspiration in Poland (Central Europe). Nat Hazards 81:55–69. doi:10.1007/s11069-015-2066-2

Borge R, Lumbreras J, Vardoulakis S, Kassomenos P, Rodriguez E (2007) Analysis of long-range transport influences on urban PM10 using two-stage atmospheric trajectory clusters. Atmos Environ 41:4434–4450. doi:10.1016/j.atmosenv.2007.01.053

Bunn AG, Goetz SJ, Fiske GJ (2005) Observed and predicted responses of plant growth to climate across Canada. Geophys Res Lett 32(16):L16710. doi:10.1029/2005GL023646

Burada DC (2013) Variabilitatea climatica in Oltenia in corelatie cu tipurile de circulatie atmosferica la scara sinoptica. PhD. Thesis, University of Bucharest

Carabaño MJ, Logar B, Bormann J, Minet J, Vanrobays M-L, Díaz C, Tychon B, Gengler N, Hammami H (2016) Modeling heat stress under different environmental conditions. J Dairy Sci 99(5):3798–3814

Carlson TN, Ripley DA (1997) On the relation between NDVI, fractional vegetation cover and leaf area index. Remote Sens Environ 62(3):24–252. doi:10.1016/S0034-4257(97)00104-1

Chakraborthy A, Sehgal VK (2010) Assessment of agricultural drought using MODIS derived normalized difference water index. Journal of Agricultural Physics 10:28–36

Croitoru AE (2014) Final report of the project Extreme weather events in Romania: heatwaves. Features, causes, impact (grant GTC-34025)

Croitoru AE, Piticar A, Burada DC (2015) Changes in precipitation extremes in Romania. Quaternary International xxx:1–11. doi:10.1016/j.quaint.2015.07.028

Croitoru AE, Piticar A, Dragotă CS, Burada DC (2013) Recent changes in reference evapotranspiration in Romania. Global and Planet Change 111:127–132. doi:10.1016/j.gloplacha.2013.09.004

Ćurić M (2012) Measuring system of adverse weather phenomena. Proceedings of the international conference air and water—components of the. Environment:68–73

Ćurić M, Živanović S (2013) Dependence between deficit and surplus of precipitation and forest fires. Disaster Advances 6(6):62–67

Dada OA, Li G, Qiao L, Ma Y, Ding D, Xu J, Li P, Yang J (2016) Response of waves and coastline evolution to climate variability of the Niger Delta coast during the past 110 years. J Mar Syst 160:64–80

De Martonne E (1926) Une nouvelle fonction climatologique: L'indice d'aridité. La Meteorologie. 449–458

Djordjević D, Tošić I, Unkašević M, Djurašković P (2010) Water-soluble main ions in precipitation over the southeastern Adriatic region: chemical composition and long-range transport. Environ SciPollut Res (ESPR) 17:1591–1598. doi:10.1007/s11356-010-0346-7

Draxler RR, Rolph GD (2011) HYSPLIT (HYbrid Single-Particle Lagrangian Integrated Trajectory) model access via NOAA ARL READY Website (http://ready.arl.noaa.gov/HYSPLIT.php).NOAA Air Resources Laboratory, Silver Spring, MD

Feizizadeh B, Blaschke T (2013) Urban Heat Island relations to land-use and air pollution: multiple Endmember spectral mixture analysis for thermal remote sensing. IEEE Journal of Selected topics in Applied Earth Observations and Remote Sensing 6(3):1749–1765

Herbel I, Croitoru AE, Imbroane AM, Petrea D (2015) Methods to detect atmospheric and surface heat islands in urban areas. Riscuri şi Catastrofe 17(2):7–17

Hsu Y, Holsen TM, Hopke PK (2003) Locating and quantifying PCB sources in Chicago: receptor modeling and field sampling. Environ SciTechnol 37(4):681–690

Imbroane AM, Croitoru AE, Herbel I, Rus I, Petrea D (2014) Urban heat island detection by integrating satellite image data and GIS techniques. Case study: ClujNapoca city, Romania. Proceedings of the 14th International Multidisciplinary Scientific Geoconference SGEM (14):359–366

Irimus IA (2003) GeografiaFizica a Romaniei. Casa Cartii de Stiinta, Cluj-Napoca

Kassomenos P, Vardoulakis S, Borge R, Lumbreras J, Papaloukas C, Karakitsios S (2010) Comparison of statistical clustering techniques for the classification of modeled atmospheric trajectories. TheorApplClimatol 102:1–12. doi:10.1007/s00704-009-0233-7

Katarzyna S (2013) The influence of atmospheric circulation on the occurrence of hail in the north German lowlands. TheorApplClimatol 112:363–373. doi:10.1007/s00704-012-0735-6

Lei H, Yang D, Huang M (2014) Impacts of climate change and vegetation dynamics on runoff in the mountainous region of the Haihe River basin in the past five decades. J Hydrol 511:786–799. doi:10.1016/j.jhydrol.2014.02.029

Ma Q, Wu J, He C (2016) A hierarchical analysis of the relationship between urban impervious surfaces and land surface temperatures: spatial scale dependence, temporal variations, and bioclimatic modulation. Landsc Ecol 31(5):1139

Marinică I (2006) Fenomene climatice de risc în Oltenia. PhD thesis. Institute of Geography, Romanian Science Academy. Bucuresti

Markham BL, Barker JL (1986) Landsat MSS and TM postcalibration dynamic ranges, exoatmospheric reflectance and at-satellite temperatures. EOSAT Landsat Tech Notes 1:3–8

Martin T (1968) Viticultura. Ed. Agrosilvica.Bucuresti

McKee TB, Doesken NJ, Kleist J (1993) The relationship of drought frequency and duration to time scales. Proceedings of the eighth conference on applied climatology. American Meteorological Society, Boston, pp. 179–184

Meng M, Ni J, Zong M (2011) Impacts of changes in climate variability on regional vegetation in China: NDVI-based analysis from 1982 to 2000. Ecol Res 26:421–428. doi:10.1007/s11284-011-0801-z

Nasri B, Tramblay Y, El Adlouni S, Hertig E, Ouarda TBMJ (2016) Atmospheric predictors for annual maximum precipitation in North Africa. J Appl Meteorol Climatol 55(4):1063–1076

Palmer WC (1965) Meteorological drought. U.S. Research Paper No. 45. US Weather Bureau, Washington, DC

Pan J (2016) Area delineation and spatial-temporal dynamics of urban Heat Island in Lanzhou City, China using remote sensing imagery. Journal of the Indian Society of Remote Sensing 44(1):111–127

Poissant L (1999) Potential sources of atmospheric total gaseous mercury in the St. Lawrence River valley. Atmos Environ 33(16):2537–2547. doi:10.1016/S1352-2310(98)00207-6

Radinović D, Ćurić M (2009) Deficit and surplus of precipitation as a continuous function of time. Theor Appl Climatol 98:197–200. doi:10.1007/s00704-009-0104-2

Radinovic D, Curic M (2013) Measuring system of adverse weather phenomena. (Abstract) Disaster Advances 6(3):19–23

Rolph GD (2011) Real-time Environmental Applications and Display sYstem (READY) Website (http://ready.arl.noaa.gov). NOAA AirResources Laboratory, Silver Spring, MD

Rolph GD (2016) Real-time Environmental Applications and Display sYstem (READY) Website (http://ready.arl.noaa.gov). NOAA Air Resources Laboratory, Silver Spring, MD

Roşca FC (2012) Frequency analysis of rainy and droughty months from the climatological point of view in Dolj country. Proceedings of the International Conference Air and Water – Components of the Environment: 480–487

Roşca FC (2013) Climatic dysfunctionalities observed with the aid of NDMI and SAVI indices in the Leu-Rotunda and Dabuleni Plains. Proceedings of the International Conference Air and Water – Components of the Environment: 500–507

Roşca FC, Petrea D (2014) The wind deflation from sand areas affected by atmospheric dryness: Leu-Rotunda and Dabuleni Fields (Oltenia Plain). Proceedings of the International Conference Air and Water – Components of the Environment: 157–164

Sandu I, Pescaru VI, Poiana I, et al. (2008) Clima Romaniei. Editura Academiei Romane, Bucharest

Sekertekin A, Kutoglu H, Kaya S (2016) Evaluation of spatio-temporal variability in land surface temperature: a case study of Zonguldak, Turkey. Environ Monit Assess 188(1):30. doi:10.1007/s10661-015-5032-2

Sjöstrom DJ, Welker JM (2009) The influence of air mass source on the seasonal isotopic composition of precipitation, eastern USA. J Geochem Explor 102(3):103–112. doi:10.1016/j.gexplo.2009.03.001

Sobrino JA, Jiménez-Muñoz JC, Paolini L (2004) Land surface temperature retrieval from LANDSAT TM 5. Remote Sens Environ 90:434–440

Soltani M, Molanejad M, Khoshakhlagh F, RanjbarSaadatAbadi A, Ranjbar F (2014) Synoptic and thermodynamic characteristics of 30 March–2 April 2009 heavy rainfall event in Iran. MeteorolAtmos Phys 126:49–63. doi:10.1007/s00703-014-0339-z

Sruthi S, Mohammed Aslam MA (2015) Agricultural drought analysis using the NDVI and land surface temperature data: a case study of Raichur District. International conference on water resources, coastal and ocean engineering (Icwrcoe 2015). Aquatic Procedia 4:1258–1264

Stein AF, Draxler RR, Rolph GD, Stunder BJB, Cohen MD, Ngan F (2015) NOAA's HYSPLIT atmospheric transport and dispersion modeling system. Bull Amer Meteor Soc 96:2059–2077. doi:10.1175/BAMS-D-14-00110.1

Tošić I, Unkašević M (2013) Extreme daily precipitation in Belgrade and their links with the prevailing directions of the air trajectories. Theor Appl Climatol 111:97–107. doi:10.1007/s00704-012-0647-5

Trigo RM, Sousa PM, Pereira MG, Rasilla D, Gouvelia CM (2016) Modelling wildfire activity in Iberia with different atmospheric circulation weather types. Int J Climatol 36(7 SI):2761–2778

Van De Griend AA, Owe M (1993) On the relationship between thermal emissivity and the normalized difference vegetation index for natural surfaces. Int J Remote Sens 14(6):1119–1131

Vicente-Serrano SM, Beguería S, López-Moreno JI (2010) A multi-scalar drought index sensitive to global warming: the standardized precipitation evapotranspiration index—SPEI. J Clim 23:1696–1718

White MA, Hoffman F, Hargrove WW, Nemani RR (2005) A global framework for monitoring phenological responses to climate change. Geophys Res Lett 32:L04705. doi:10.1029/2004GL021961

Xie Q, Zhou Z, Teng M, Wang P (2012) A multi-temporal Landsat TM data analysis of the impact of land use and land cover changes on the urban heat island effect. Journal of Food, Agriculture & Environment 10(2):803–809

Zhou L, Tucker CJ, Kaufmann RK, Slayback D, Shabanov NV, Myneni RB (2001) Variations in northern vegetation activity inferred from satellite data of vegetation index during 1981 to 1999. J Geophys Res 106(D17):20069–20083